Supplementary Information for

The Role of Sulfur Vacancies on FeS_2(100) for NO Dissociative Adsorption: a Combined in-situ SR-XPS and DFT Calculation

Wei-Chih Hsiao,[a] Fumihiko Ozaki, †[a] Kozo Mukai,[a] Shunsuke Tanaka,‡[a] Daisuke Nishio-Hamane,[a] Masahiro Fukuda,[a] Taisuke Ozaki,[a] and Jun Yoshinobu*[a]

[a]The Institute for solid state physics, The University of Tokyo, Chiba, 2770882, Japan.
† Present address: Research and Development Directorate, Japan Aerospace Exploration Agency (JAXA), Sagamihara, Kanagawa, 2525210, Japan.

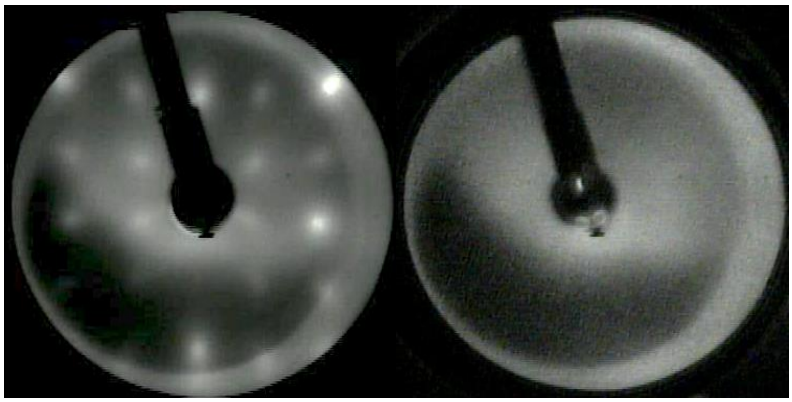

Fig S1. (1×1) LEED pattern of the low-S_{vac} **(left)**, and high-S_{vac} **(right)** FeS_2(100) surfaces, recorded at an electron beam energy of 110 eV.

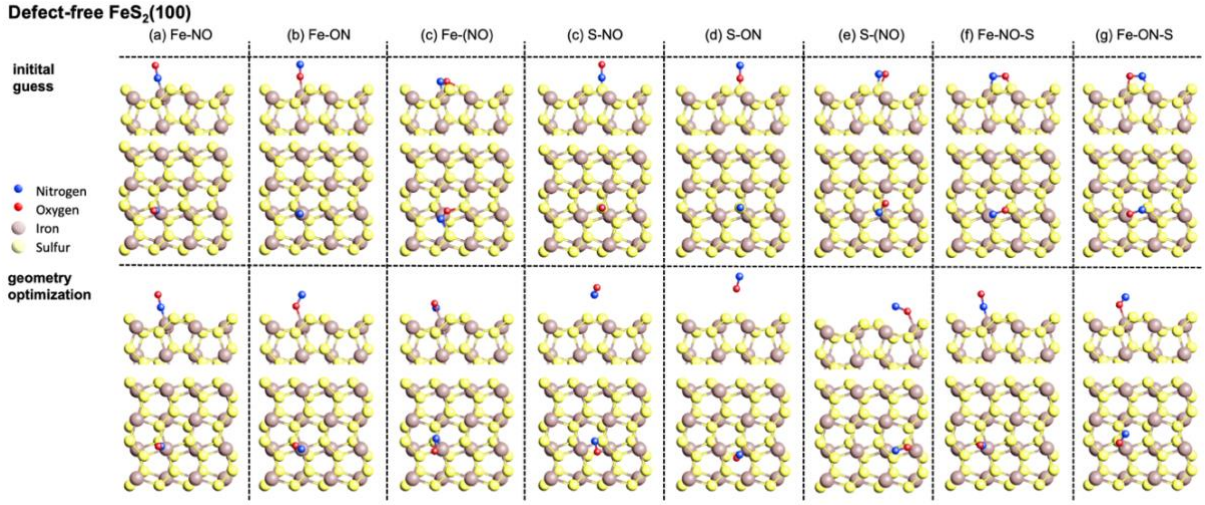

Fig S2. Side view (upper) and top view (lower) of optimized geometries of defect-free FeS_2(100) surfaces for various adsorbate configurations. Top and bottom rows represent the initial adsorption geometries and the structures after geometry optimization, respectively. Color scheme: nitrogen (blue), oxygen (red), iron (brown), and sulfur (yellow).

Table S1. Calculated adsorption energy (ΔE_{ads}), N–O bond length (d(N–O)), and charge transfer (ΔQ, Mulliken analysis) for NO adsorption on defect-free FeS_2(100) surfaces with different initial adsorption configurations on defect-free FeS_2(100) surfaces. The most stable configurations are highlighted in red.

Initial gauss	ΔE_{ads} (eV)	d(N-O)	ΔQ of NO (e)
Fe-NO	-2.01	1.19	0.09
Fe-ON	-0.95	1.22	0.15
Fe-(NO)	-0.94	1.19	0.19
S-NO	-0.40	1.20	0.09
S-ON	-0.23	1.20	0.05
S-(NO)	-0.37	1.21	0.08
Fe-NO-S	-2.01	1.19	0.08
Fe-ON-S	-0.93	1.22	0.15

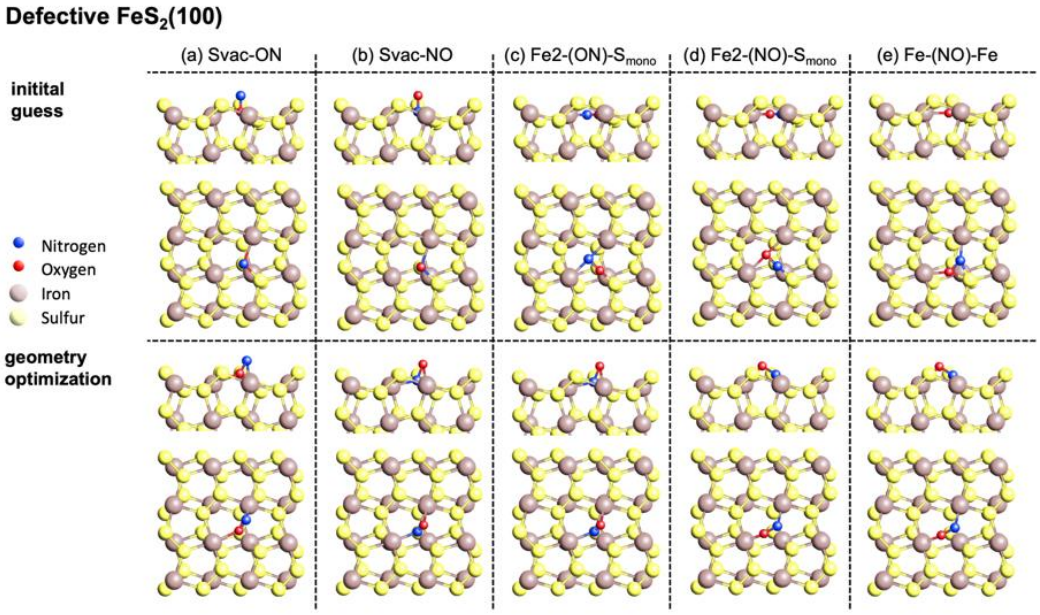

Fig S3. Side view (upper) and top view (lower) of optimized geometries of defective FeS_2(100) surfaces with a sulfur vacancy (Svac) for various NO adsorption configurations. Top and bottom rows represent the initial adsorption geometries and the structures after geometry optimization, respectively. Color scheme: nitrogen (blue), oxygen (red), iron (brown), and sulfur (yellow).

Table S2. Adsorption energy (ΔE_{ads}), N–O bond length (d(N–O)), and charge transfer (ΔQ, Mulliken analysis) for NO adsorption on defective FeS_2(100) surfaces with a sulfur vacancy (Svac) in various configurations on defective FeS_2(100) surfaces. The most stable configurations are highlighted in red.

Initial gauss	ΔE_{ads} (eV)	d(N-O)	ΔQ of NO (e)
Svac-ON	-1.75	1.29	0.37
Svac-NO	-3.09	1.31	0.40
Fe2-(ON)-S_{mono}	-3.10	1.31	0.39
Fe2-(NO)-S_{mono}	-2.86	1.27	0.35
Fe-(NO)-Fe	-2.84	1.27	0.36

The sulfur-vacancy formation energies for the FeS_2(100) surface were calculated, and we obtained ΔH = 0.12 eV based on eqn (1) and 0.09 eV based on eqn (2). These values suggest that sulfur-vacancy formation is thermodynamically accessible. We note that in our experiments sulfur vacancies were mainly created by Ar^+ sputtering (non-thermal process).

FeS_2 (non-defect) → FeS_2 (with one S_{vac}) + $1/2S_{2(isolated)}$ (1) ΔH = 0.12 eV

FeS_2 (non-defect) → FeS_2 (with one S_{vac}) + $1/8S_{8(solid)}$ (2) ΔH = 0.09 eV

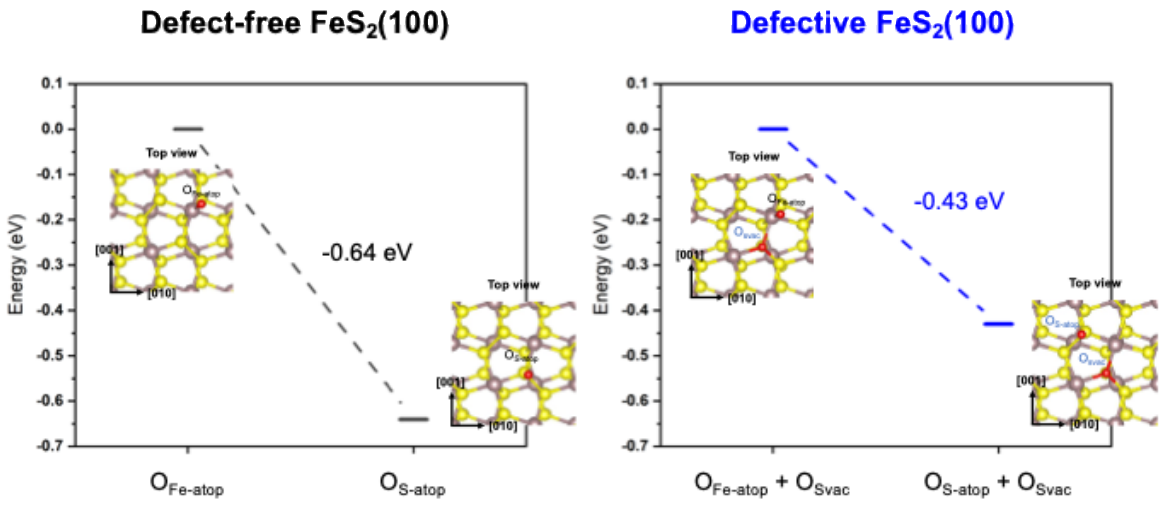

Fig S4. DFT-D3 calculated relative stabilities of atomic oxygen adsorbed at Fe-atop and S-atop sites on defect-free and defective FeS_2(100) surfaces. On both surfaces, oxygen adsorption at the S-atop site is energetically more favourable than at the Fe-atop site, with energy differences of −0.64 eV for the defect-free surface and −0.43 eV for the defective surface. Representative optimized adsorption geometries are shown as insets.

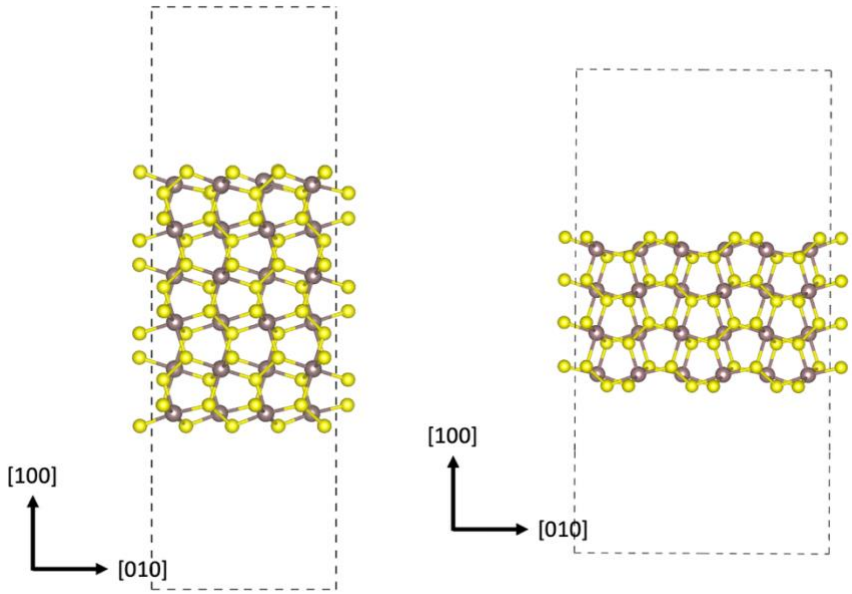

Fig S5. DFT-D3 calculated (3 × 2 × 2) slab model for geometry optmizations **(left)** and (2 × 3 × 3) slab model for absolute binding energy calculations **(right)**